

Fig. 1. Energy band diagrams of 2D Dirac-source cold electron injection in a Gr/MoS₂ heterobilayer. Here E is the energy, DOS is the density of states, n is the carrier concentration, E_{C} is the conduction band edge, and E_{F} is the Fermi level. The Gr-enabled cold source injection has a short thermal tail terminated at the Dirac point energy level (E_{Dirac}), and can be cut off more efficiently by a gate-controlled potential barrier ϕ_{b} at the van der Waals (vdW) interface.

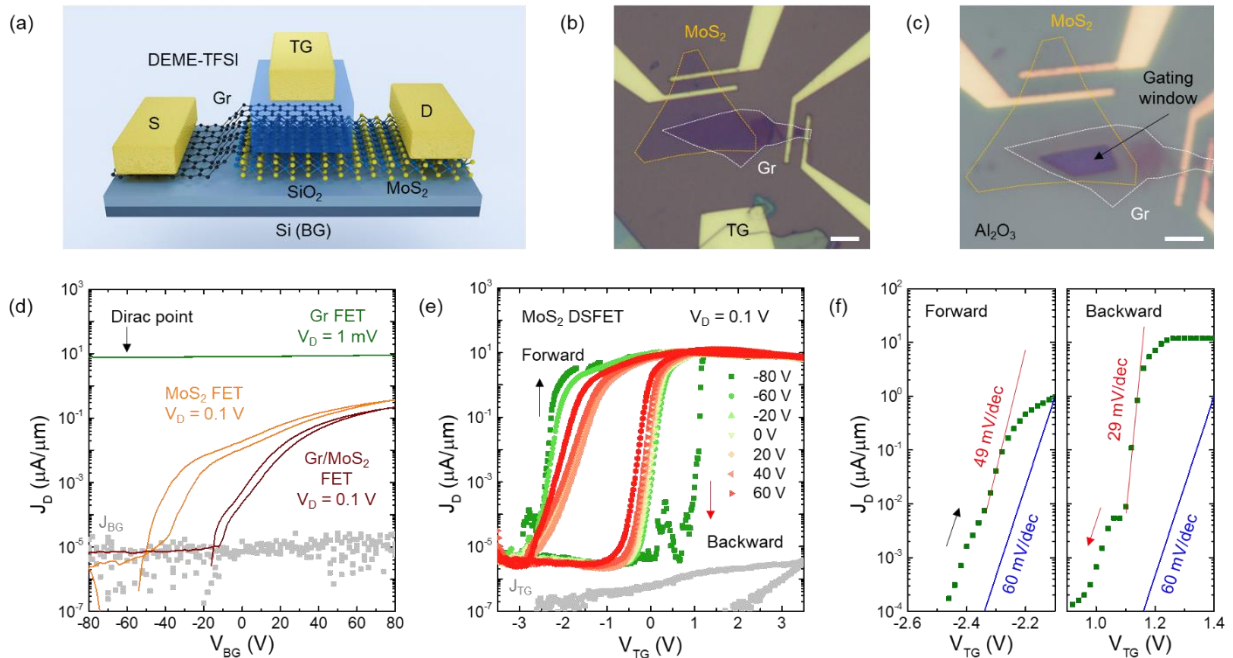


Fig. 2. (a) Schematic illustration of a 2D MoS₂ CSFET. (b, c) Optical microscopy images of the device before and after Al₂O₃ deposition. (d) $J_{\text{D}} - V_{\text{BG}}$ transfer characteristics of the back-gate Gr FET, MoS₂ FET, and Gr/MoS₂ FET. J_{BG} is the back-gate leakage current density. (e) $J_{\text{D}} - V_{\text{TG}}$ transfer characteristics of the top-gate MoS₂ CSFET. J_{TG} is the top-gate leakage current density. Black and red arrows indicate the forward and backward sweeps, respectively. (f) Sub-60-mV/decade switching at $V_{\text{BG}} = -80 \text{ V}$ in the forward and backward sweeps. Blue line is the 60 mV/decade thermionic limit.

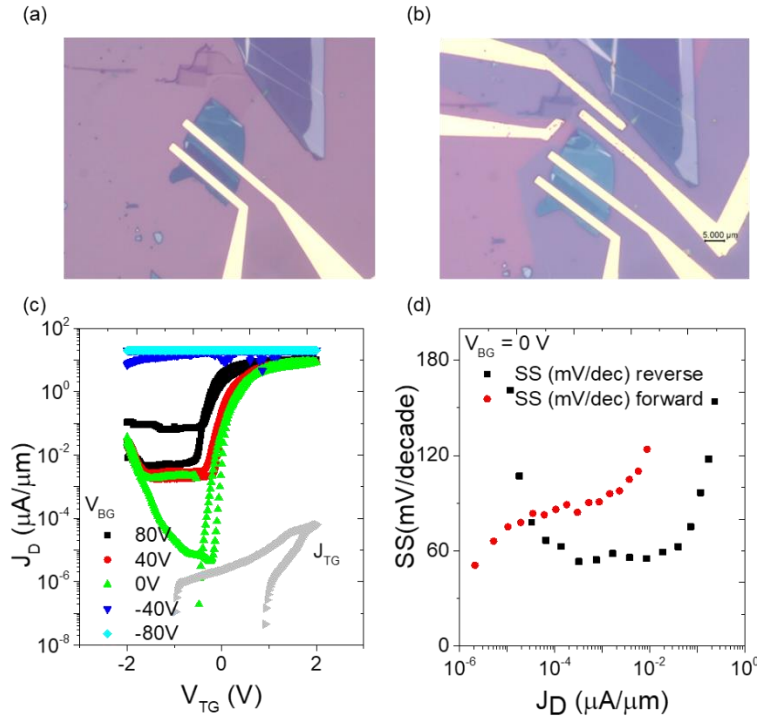


Fig. 3. (a, b) Optical microscopy images of the WSe₂ CSFET device before and after Al₂O₃ deposition. (c) J_D - V_{TG} transfer characteristics of the top-gate WSe₂ CSFET. (d) SS as a function of J_D at $V_{BG} = 0$ V in the forward and backward sweep.

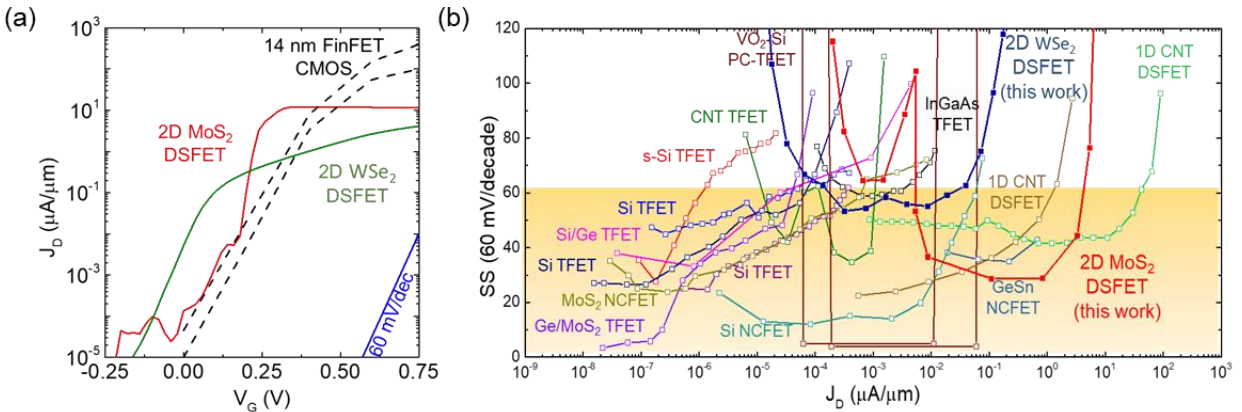


Fig. 4. (a) Transfer characteristics of 2D MoS₂ and WSe₂ CSFETs in a comparison with 14 nm FinFET CMOS technology. (b) SS as a function of J_D in a comparison with TFETs, NCFETs, and 1D CSFETs based on a variety of channel materials.